JACS
JOURNAL OF THE AMERICAN CHEMICAL SOCIETY
Article
pubs.acs.org/JACS

Inverse-Micelle-Encapsulated Water-Enabled Bond Breaking of Dialkyl Diselenide/Disulfide: A Critical Step for Synthesizing High-Quality Gold Nanoparticles

Oksana Zaluzhna,[†] Ying Li,[†,§] Thomas C. Allison,[‡] and YuYe J. Tong*[,†]

[†]Department of Chemistry, Georgetown University, 37th and O Streets NW, Washington, D.C. 20057, United States
[‡]National Institute of Standards and Technology, 100 Bureau Drive, Gaithersburg, Maryland 20899-8320, United States

Supporting Information

ABSTRACT: Inverse-micelle-encapsulated water formed in the two-phase Brust–Schiffrin method (BSM) synthesis of Au nanoparticles (NPs) is identified as essential for dialkyl diselenide/disulfide to react with the Au(III) complex in which the Se–Se/S–S bond is broken, leading to formation of higher-quality Au NPs.

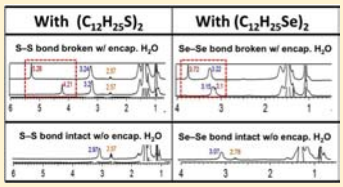

INTRODUCTION

The popular Brust–Schiffrin[1] (BSM) procedure has been widely used to synthesize thiolate-protected Au NPs. Its profound impact on making modern metal NPs in general and on inspiring their many promising novel applications can hardly be overstated.[2−6] Moreover, several recent studies have also made great strides in our mechanistic understanding of the chemistry of metal NP formation in terms of identifying the Au precursors and the reaction microenvironment.[7−10] Particularly, Goulet and Lennox[10] have discovered that a stoichiometric Au complex involving cations of the Au-ion-transferring surfactant (i.e., TOA^+, tetraoctylammonium cation), $[TOA][Au(III)X_4]$, is formed during the phase-transfer in a BSM synthesis, which is further reduced to $[TOA][Au(I)X_2]$ without forming the generally accepted polymeric $Au(SR)_n$ after the addition of thiols to the separated organic phase. Later, Li et al. have established that inverse micelles are formed in the separated organic phase to host the Au complex[7] and the inverse-micelle-encapsulated water provides a favorable hydrophilic micro-environment as a proton-accepting medium for the cleaved thiol protons[11] that may also lead to the H_2 formation.[12,13]

On the other hand, when dialkane disulfide is used in lieu of alkanethiols as the starting ligand in the BSM synthesis, Au NPs can also be formed. As a matter of fact, the first reported self-assembled monolayer on Au was achieved with a disulfide ligand.[14] In both cases, disulfide bond breaking is a necessary step, but its mechanism is still largely unknown. Moreover, if selenium (Se) is to be used as an alternative to sulfur for anchoring molecular wires for better electrical conductance, one is highly likely to use diselenide ligands because of the instability of alkylselenol in air.[15,16] Therefore, unraveling the detailed chemistry of S–S and Se–Se (or dichalcogenide in general) bond breaking in the formation of metal NPs and its relationship with encapsulated water in the context of the BSM two-phase synthesis of Au NPs is an important and timely subject and the focus of this article. For this purpose, we carried out a comparative study by using both dialkyl diselenide and dialkyl disulfide as the sources of protecting ligand. We discovered that it is the inverse-micelle-encapsulated water that enables uniquely the breaking of the diselenide or disulfide bond and the formation of a likely Au(II) complex, which is a step that is essential in forming high-quality Au NPs.

EXPERIMENTAL SECTION

Chemicals. Didodecyl disulfide was synthesized according to the modified literature procedure.[17] To a solution of 2.4 mL of $C_{12}H_{25}SH$ and 30 mL of ethyl acetate, 15 mg of NaI was added. After the addition of 1.1 mL of 30 wt % H_2O_2, the mixture was stirred at room temperature for 30 min. To the clear yellow solution, 15 mL of $Na_2S_2O_3$ (3.13 g) aqueous solution was added, leading to a fading of the color of the solution. The two-phase mixture was transferred to a separatory funnel. After removal of the solvent from the top solution, the desired product was obtained as a white crystalline powder.

Didodecyl diselenide was synthesized according to the modified literature method.[18] An additional purification step was included at the end, where solution was run through a silica/hexanes column (60 cm in length and 6 cm in diameter) to purify the product. The yellow band was collected and rotary evaporated to obtain yellow solid product.

$[TOA][AuBr_4]$ was synthesized according to the literature.[10,19] TOAB (1.26 g) and $KAuBr_4 \cdot H_2O$ (1.37 g) were mixed with 60 mL of anhydrous EtOH. After 1 h of stirring and 10 min of sonication, the mixture was stored in a freezer overnight. The expected product was collected through vacuum filtration.

Au Intermediates and Nanoparticles Synthesis. The steps of a BSM two-phase synthesis of Au NPs used here are as follows: (1) phase transfer of Au(III) from the aqueous solution of $HAuCl_4$ to the organic (benzene) phase by the surfactant tetraoctylammonium bromide (TOAB) that involves the formation of complex $[TOA][Au(III)X_4]$, (2) separation of the organic phase after complete Au(III) transfer in order to better control the amount and therefore delineate the effect of water, (3) addition of the ligand (dialkyl

Received: July 14, 2012
Published: October 9, 2012

   dx.doi.org/10.1021/ja3068758 | J. Am. Chem. Soc. 2012, 134, 17991−17996

disulfide or dialkyl diselenide) to the separated organic phase, and (4) mixture of the $NaBH_4$ aqueous solution (all at once) with the organic solution of step 3 to reduce Au cations to Au(0) through which Au NPs are formed. We will first focus on identifying chemical species involved in steps 2 and 3 by ^{1}H NMR and Raman spectroscopies, aided by ab initio density functional theory (DFT) calculations for the assignments of vibrational bands observed by Raman.

For the ^{1}H NMR study, the following intermediate solutions were prepared: 0.0164 g of TOAB was dissolved in 0.5 mL of C_6D_6, to which 0.189, 0.0949, or 0.0649 mL of $HAuCl_4$ aqueous solution (0.158 M) was added to form solutions of TOAB/Au ratios of 1:1, 2:1, and 3:1, respectively. After the aqueous layer turned colorless indicating that all Au(III) ions were transferred into the organic phase, the wine-red top organic layer was collected, and 0.5 equiv of $(C_{12}H_{25}S)_2$ or $(C_{12}H_{25}Se)_2$ (i.e., Au/(S or Se) = 1:1) was added. (Note that in ref 16 the separation of organic layer was done *after* the addition of ligands and a subsequent overnight stirring in which the color change was observed.) The reference intermediate solution was made by dissolving the $[TOA][AuBr_4]$ complex directly in C_6D_6 with addition of 2 equiv of TOAB and 0.5 equiv of dichalcogenides. This ensured that *no water* was present and the organic solution had a final ratio of TOAB/Au of 3:1. All the (*separated*) organic solutions were stirred for 2 h and then analyzed by ^{1}H NMR. For the Raman studies, the corresponding concentrated solutions were obtained by evaporating the solvent from the given organic solution, dropping a sample on a clean glass slide, and drying it in air overnight. Note that *no* obvious color change was observed for both dichalcogenides after a 2 h stirring (see insets in Figure 5). However, both the NMR and Raman data suggest that certain reactions/interactions between the ligands and Au ions did take place.

Characterizations. *NMR.* ^{1}H NMR spectra were recorded on a Bruker/Tecmag AM 300 MHz spectrometer that was interfaced with a Tecmag DSPect acquisition system. Deuterated benzene was used as solvent, whose ^{1}H peak (7.16 ppm) was used as the secondary reference. The OriginPro8 program was used for integration.

Raman Spectroscopy. Spectra were obtained using a confocal microprobe Raman system (Renishaw RM1000) equipped with a deep depletion CCD Peltier cooled to −70 °C. The microscope attachment was based on an Olympus BH2-UMA system, and a 50×-long working-length objective (8 mm) was used. A holographic notch filter was used to filter the exciting line, and two selective holographic gratings (1200 and 2400 g/mm) were employed with respect to the required spectral resolution. The exciting wavelength was 785 nm from the diode laser with a maximum power of 27 mW and a spot of ~3 μm on the surface. The slit and pinhole in the experiment were 100 and 400 μm, respectively. The spectroscopy was calibrated with the peak of a clean Si wafer at 520 cm^{-1}. The liquid sample was measured in a 5 mm NMR tube. Solid or slurry samples were measured on a clean microscope slide.

Electrochemistry. The electrochemical measurements were performed in an Ar-blanketed conventional three-electrode cell using a CHI 760C potentiostat (CH Instrument, Inc.) that was controlled by a computer with the CHI software. Commercial Ag/AgCl (3M; CH Instrument, Inc.) and Pt gauze electrodes were used as the reference and counter electrodes, respectively. The working electrode comprised a well-polished 3 mm commercial glassy carbon electrode (BASi). The supporting electrolyte was an ACN solution (10 mL) of 0.1 M tetrabutylammonium perchlorate. Cyclic voltammograms (CVs) were recorded with a 50 mV/s scan rate. A blank electrode was run first as a reference, then the proper amount of each intermediate that led to a final 0.2 mM Au concentration was added to the supporting electrolyte, and the stabilized OCP (open circuit potential, within 500 s) and CV of the given sample were collected respectively.

UV–Visible. A UV–vis spectrometer with HP 8453 diode array was used for measurements. The intermediates were dissolved in benzene, and the resultant solution was placed in a 1 cm path length quartz cuvette for measurement in the spectral range of 200–800 nm.

DFT Calculations. Calculations were carried out at the B3LYP/cc-pVDZ level of theory (the cc-pVDZ-PP pseudopotential basis set was used on Au) using the GAMESS quantum chemistry program.[20] All structures were fully optimized at the stated level of theory. Vibrational frequencies were computed using two-sided numerical differencing of the analytic gradient, and a scaling factor of 0.97 was used.[21] Calculations were carried out on $[HAuBr4](SeC_4H_9)_2$ and Au(III)-$(SeC_4H_9)_2$. Our experience has shown that the butyl chains used in this study are a very good substitute for the longer (and computationally more demanding) chains used in the experimental work. The use of this smaller chain has a negligible effect on the resulting vibrational frequencies.

RESULTS AND DISCUSSION

We begin by describing the didodecyl diselenide, $(C_{12}H_{25}Se)_2$, system. The ^{1}H NMR spectra of the intermediate solutions obtained after the addition of diselenide, together with spectra of some reference materials, are shown in Figure 1. Curves a–c

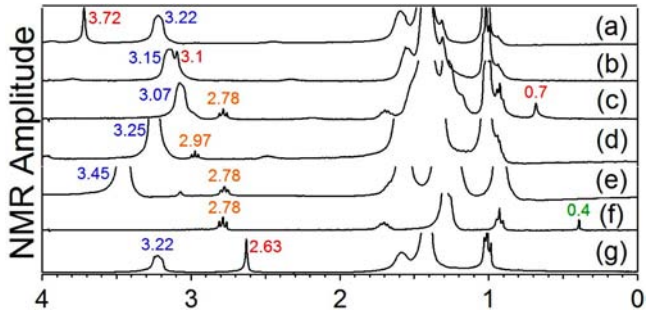

Figure 1. ^{1}H NMR spectra of the intermediate solutions with the same Au/Se ratio of 1:1 but different TOAB/Au ratios of (a) 3:1 (TAuSe-311), (b) 2:1 (TAuSe-211), and (c) 1:1 (TAuSe-111) and (d) 3:1 but with $[TOA][AuBr_4]$/2TOAB/0.5$(C_{12}H_{25}Se)_2$ (TAuSe-311C) and of reference materials (e) 3TOAB/0.5$(C_{12}H_{25}Se)_2$ (TAuSe-301), (f) $(C_{12}H_{25}Se)_2$ (TAuSe-001), and (g) 3TOAB/1$HAuCl_4$ (TAuSe-310), all in C_6D_6.

of Figure 1 are the spectra of the intermediate solutions after adding diselenide to the *separated* organic phase-transferred layer with Au/Se of 1:1 but with TOAB/Au of 3:1, 2:1, and 1:1, respectively. Figure 1d is the spectrum obtained by adding $(C_{12}H_{25}Se)_2$ to a C_6D_6 solution of preformed $[TOA][AuBr_4]$ complex plus 2 equiv of TOAB, yielding TOA/Au of 3:1. Curves e–g of Figure 1 are references: those of the simple mixture of TOAB/$(C_{12}H_{25}Se)_2$ of 3:1, pure $(C_{12}H_{25}Se)_2$, and the organic solution after the complete Au(III) phase transfer with TOAB/Au of 3:1. All these solutions were prepared using C_6D_6 as solvent. Since about a dozen samples will be discussed, we will name the samples as TAu[Se/S]-*lmn*(C) to simplify their description and facilitate discussion. Here T represents the surfactant TOAB, C describes the situation when the $[TOA][AuBr_4]$ complex was used in preparing the intermediate, and *lmn* represent numbers that give the atomic ratio of the surfactant (TOAB), the metal (Au), and the chalcogen (Se or S) in the sample. A zero means the absence of that ingredient. For instance, TAuSe-311C stands for a sample prepared with $[TOA][AuBr_4]$ complex (C) and the final ingredients ratio is TOAB/Au/Se of 3:1:1.

In Figure 1, the triplet peaks at 2.78 ppm (orange) belong to the α-CH_2Se– protons of $(C_{12}H_{25}Se)_2$ (Figure 1f, TAuSe-001). Those indicated by the blue numbers arise from the α-CH_2N^+ protons of TOAB (whose variation, also observed in Figure 3, was caused by the presence of Au ions and changes in their oxidation state and in acidity of the encapsulated water[11]), and those indicated by red numbers come from encapsulated water with acidic protons (3.72 ppm in Figure 1a, TAuSe-311, and

dx.doi.org/10.1021/ja3068758 | J. Am. Chem. Soc. 2012, 134, 17991–17996

3.10 ppm in Figure 1b, TAuSe-211). Figure 1g (TAuSe-310) reproduces exactly what was observed previously,[11] and the 2.63 ppm peak came from the inverse-micelle-encapsulated water. It was also observed previously[11,22] that TAuSe/S-210 encapsulates water but not TAuSe/S-110.

As expected, no reaction between the surfactant and ligand occurred by simply mixing them together (TAuSe-301) (Figure 1e). Neither reaction occurred between the surfactant, Au ions, and ligand in TAuSe-311C (Figure 1d) in which *no water* was present, although the presence of the Au(III) complex did shift the peak at 2.78 ppm to 2.97 ppm without changing its triplet line shape. This suggests the possible formation of a Lewis adduct between diselenide and Au ions without the Se−Se bond being broken. However, if the ligand was added to the post-Au(III)-transferred organic solution where inverse-micelle-encapsulated water existed, i.e., TAuSe-310 (Figure 1g) and TAuSe-210, the reaction took place as evidenced by the appearance of the acidic proton peaks at 3.72 and 3.1 ppm and the complete disappearance of the peaks at 2.78 ppm in Figure 1a (TAuSe-311) and Figure 1b (TAuSe-211), respectively. The latter indicates that all Se−Se bonds were broken. What is striking is that no evidence of reaction was observed in Figure 1c (TAuSe-111) where no encapsulated but freelike water (0.7 ppm peak) was observed.

The corresponding Raman spectra of Figure 1 are shown in Figure 2. Figure 2g (TAuSe-310) is a simple addition of the

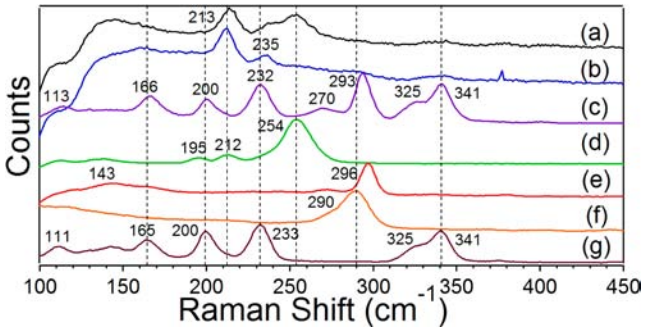

Figure 2. Raman spectra of the concentrated intermediate solutions of those in Figure 1. The dashed vertical lines are used to identify similar bands. See Figure S1 in Supporting Information for corresponding full Raman spectra.

spectra of individual components: TOAB and $HAuCl_4$. Clearly no reaction occurred between them. As observed previously, the diselenide stretching band in the presence of TOAB showed a 6 cm^{-1} (TAuSe-301, Figure 2e) positive shift compared to that (290 cm^{-1}) in Figure 2f (TAuSe-001), although no shift was observed in the α-CH_2Se− proton peak (Figure 1e). The latter observation convinced us that no reaction took place between diselenide and TOAB in TAuSe-301. That is, the Se−Se bond was intact.

Interestingly, when diselenide was added to the Au complex solution *without* water (TAuSe-311C), the Raman spectrum changed dramatically: an intense band at 254 cm^{-1} was observed in addition to two much weaker bands at 195 and 212 cm^{-1} that can be assigned to the $[AuBr_4]^-$ moiety. In order to identify the intense band at 254 cm^{-1}, since NMR (Figure 1d) strongly suggests that the Se−Se bond was most likely not broken, DFT (density functional theory) calculations were carried out on two candidate molecular structures whose optimized molecular structures are shown in Figure S3 of the Supporting Information. (The candidate structures listed gave the best agreement with the experimental measurements out of many possible structures that were considered.) For the $[HAu(III)Br_4]$ $(SeC_4H_9)_2$ structure, the calculated (scaled) Se−Se stretching frequency is 281 cm^{-1} but is 260 cm^{-1} for the $Au(III)(SeC_4H_9)_2$ structure. Therefore, we assigned the band at 254 cm^{-1} to a $Au(III)(SeC_4H_9)_2$-like species, which is consistent with the positive ^1H NMR peak shift (Figure 1d) that can be rationalized by the interaction with electron withdrawing Au(III). Equally interesting is that Figure 2c (TAuSe-111) appears to also be a simple addition of Figure 2g (TAuSe-310) and Figure 2f (TAuSe-001), suggesting strongly that no reaction between diselenide and the Au complex took place despite the presence of nonencapsulated water (0.7 ppm peak in Figure 1c), in agreement with the NMR observation. Moreover, no obvious change in the bands from $[AuCl_4]^-$ (325 and 341 cm^{-1}) and no bands from $[AuBr_4]^-$ (195 and 212 cm^{-1}) were observed in Figure 2c (TAuSe-111), which suggests that no major replacement of Cl^- by Br^- in the $[AuX_4]^-$ moiety took place with TOAB/Au of 1:1.

On the other hand, a reaction did occur between the ligand and metal cation once the inverse-micelle-encapsulated water was present (TAuSe-311 and -211), as evidenced by the complete disappearance of the Se−Se bonds, i.e., the complete disappearance of the Se−Se stretching band in Figure 2a and Figure 2b and α-CH_2Se− proton peak in Figure 1a and Figure 1b. Also, significant displacement of Cl^- by Br^- occurred as evidenced by the appearance of the 213 cm^{-1} band from $[AuBr_4]^-$ and the substantial decrease of the bands (325 and 341 cm^{-1}) from $[AuCl_4]^-$. Therefore, per the above observations, we conclude that *the presence of inverse-micelle-encapsulated water enabled the bond-breaking* reaction *between diselenide and the Au(III) complex.*

We also investigated the dialkyl disulfide for purposes of comparison. The ^1H NMR spectra of the intermediate solutions under the same conditions as those in Figure 1, replacing dialkyl diselenide with dialkyl disulfide, are shown in Figure 3. As in Figure 1, the peaks at 2.57 ppm (orange) in Figure 3 belong to the protons of α-CH_2S− of TAuS-001 (Figure 3f). Those indicated by the blue numbers arise from the protons of α-CH_2N^+ of TOAB, and those by red numbers come from the encapsulated water with (Figure 3a, TAuS-311; Figure 3b, TAuS-211) or without (Figure 3g, TAuS-310) acidic protons.

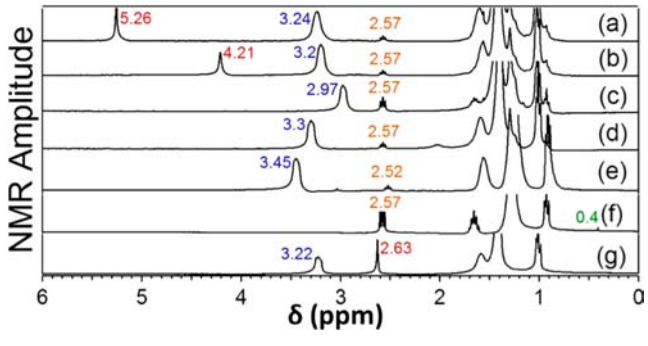

Figure 3. ^1H NMR spectra of the intermediate solutions with the same Au/S ratio of 1:1 but different TOAB/Au ratios of (a) 3:1 (TAuS-311), (b) 2:1 (TAuS-211), and (c) 1:1 (TAuS-111) and (d) 3:1 but with $[TOA][AuBr_4]$/2TOAB/0.5 $(C_{12}H_{25}S)_2$ (TAuS-311C) and of reference materials (e) 3TOAB/0.5$(C_{12}H_{25}S)_2$ (TAuS-301), (f) $(C_{12}H_{25}S)_2$ (TAuS-001), and (g) 3TOAB/1$HAuCl_4$ (TAuS-310), all in C_6D_6.

dx.doi.org/10.1021/ja3068758 | J. Am. Chem. Soc. 2012, 134, 17991−17996

Figure 3g is the same spectrum as Figure 1g, reproduced here for reference.

As in the case of diselenide, no reaction occurred between TOAB and the ligand by simply mixing them (TAuS-301) (Figure 3e). Neither reaction occurred between the TOAB, metal ion, and ligand in TAuS-311C with *no water* present (Figure 3d). No shift of the 2.57 ppm peak was observed in this case, indicating that little interaction, if any, between disulfide and the Au complex existed, *unlike* the case of diselenide (TAuSe-301) where the formation of a Lewis adduct was inferred (Figure 1d, Figure 2d, and the DFT calculations). As observed for the Se case, the presence of inverse-micelle-encapsulated water in the post-Au(III)-transferred organic solution immediately enabled the reaction between disulfide and Au complex in TAuS-311 and -211, as implied by the appearance of the acidic proton peaks at 5.26 and 4.21 ppm in Figure 3a and Figure 3b, respectively. However, in contrast to the case of diselenide, the reaction did not consume all the starting disulfide because the peak at 2.57 ppm still remained, although with substantially decreased amplitude.

The corresponding Raman spectra of the solutions in Figure 3 are presented in Figure 4. Figure 4g is a reproduction of

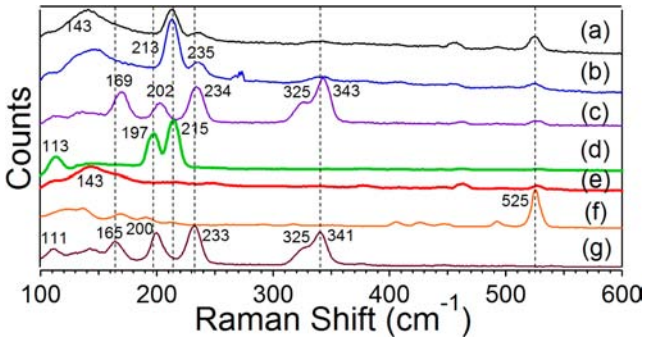

Figure 4. Raman spectra of the concentrated intermediate solutions analogous to those in Figure 3. The dashed vertical lines are used to identify similar bands. See Figure S2 in Supporting Information for corresponding full Raman spectra.

Figure 2g for reference. Figure 4d shows a simple addition of disulfide to the C_6D_6 solution of $[TAO][AuBr_4]$ (TAuS-311C), though the S−S band at 525 cm^{-1} is tiny compared to the intense peaks at 197 and 215 cm^{-1} from the $[AuBr_4]^-$ moiety. This suggests that the disulfide did not interact strongly (if at all) with the Au complex, consistent with the conclusion reached based on the ^{1}H NMR (Figure 3d). This is in great contrast to the case of diselenide where the possible formation of a Lewis adduct was inferred (Figure 1d and Figure 2d). As in Figure 2c (TAuSe-111), Figure 4c (TAuS-111) appears to be a simple addition of the spectra of the individual components, TAuS-310 (Figure 4g) and TAuS-001 (Figure 4f), with no evidence of reaction between the disulfide and the Au complex but with evidence (vide supra) indicating that no major displacement of Cl^- by Br^- took place. On the other hand, Figure 4a (TAuS-311) and Figure 4b (TAuS-211) show that significant change occurred once inverse-micelle-encapsulated water was present. That is, a reaction took place as in the case of diselenide (Figure 2a and Figure 2b), although the remaining S−S vibrational band at 525 cm^{-1} in Figure 4a and Figure 4b (also the 2.57 ppm peak in Figure 3a and Figure 3b) indicates that not all original ligands were consumed.

As in the cases of diselenide (vide supra), results obtained on disulfide show again that inverse-micelle-encapsulated water was *indispensable* for the reaction of disulfide with the Au complex. What was intriguing in both cases is that no obvious color change was observed (see insets in Figure 5), suggesting

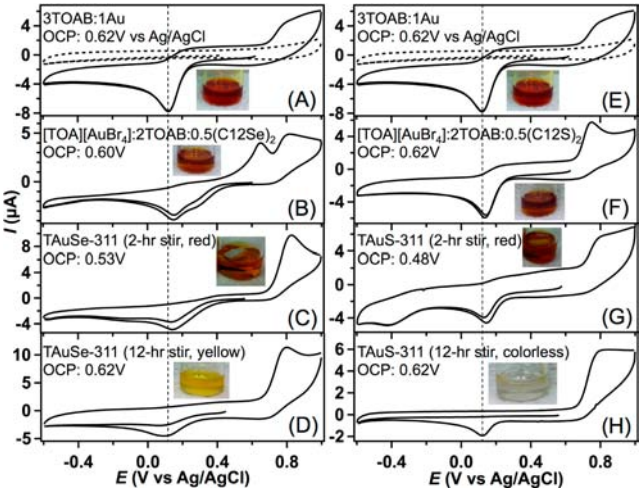

Figure 5. Cyclic voltammetric measurements of the samples: (A) TAuSe-310, (B) TAuSe-311C (no encapsulated water), (C) TAuSe-311, (D) TAuSe-311 (stirred in open air), (E) TAuS-310 (the same as in part A, reproduced here as a reference for samples involving disulfide), (F) TAuS-311C (no encapsulated water), (G) TAuS-311, and (H) TAuS-311 (stirred in open air). The insets in parts A–H show the color of the corresponding solutions. The corresponding representative OCP (open circuit potential) values are also shown. The samples D and H were obtained by stirring samples C and G, respectively, in the open air for 12 h. The products of the same respective color as samples D and H would have been obtained if no separation of aqueous phase was done after the phase transfer as in ref 22.

that the Au(III) was not reduced to Au(I) because the latter would be colorless but rather to a different species that could highly likely be the rarely observed Au(II) whose color was indeed observed to be reddish.[23] While our ESR measurements have so far been unsuccessful to observe signals from the expected paramagnetic Au(II) species, preliminary electrochemistry (Figure 5) and UV characterizations (Figure 6) did at least ascertain that the species were not Au(III) or Au(I).

The difference between the CVs in Figure 5B and Figure 5F, i.e., identical reduction peaks in Figure 5F vs 5E but different peaks in Figure 5B vs 5A, is consistent with the different interaction between disulfide and diselenide with the Au(III) cations discussed above. That is, no interaction was observed for the former when no encapsulated water was present. On the other hand, that no or little reduction current was observed in the first negative potential scan in Figure 5D and Figure 5H indicates the dominant presence of Au(I) because the reduction of Au(I) to Au(0) takes place at further negative potential. Moreover, the much lower OCPs for samples C and G compared to those of others imply strongly that they were different Au cations from Au(III) (Figure 5B and Figure 5F) or Au(I) (Figure 5D and Figure 5H), likely Au(II).

That the oxidation state of the Au cations in TAuSe-311/TAuS-311 after only 2 h of stirring was different from that of either Au(III) or Au(I) is further confirmed by the UV–vis data as shown in Figure 6. The blue (for the sample with no ligand) and green (for the sample with ligand but with no encapsulated

dx.doi.org/10.1021/ja3068758 | J. Am. Chem. Soc. 2012, 134, 17991–17996

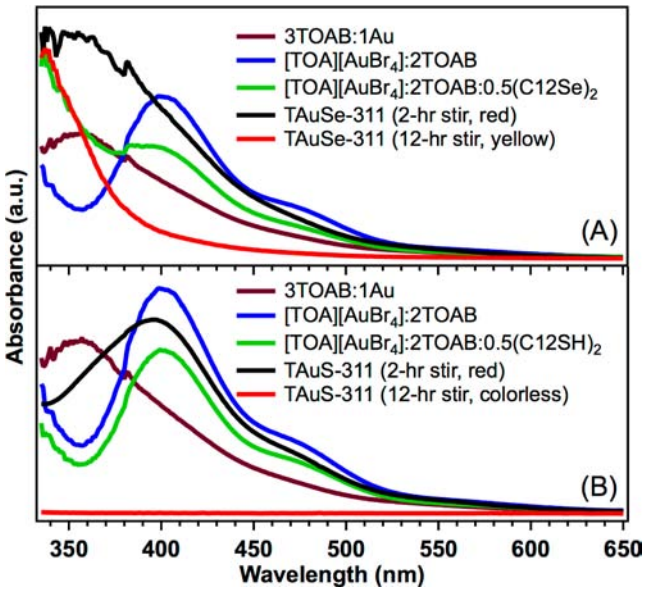

Figure 6. UV−vis spectra of the same samples studied by electrochemistry in Figure 5: (A) for diselenide system and (B) for disulfide system.

water) curves are of different line shape in part A but identical in part B. This implies a strong interaction between diselenide and Au(III) but (almost) no interaction between disulfide and Au(III) when no encapsulated water was present, in agreement with the conclusion reached from NMR, Raman, and electrochemistry measurements discussed above. The black curves in parts A and B, presumably from Au(II), are clearly different from the rest of the curves, particularly in part B, which indicates again the existence of the Au cations that were different from Au(III) or Au(I).

Since no viable proton sources other than water existed in the reaction solutions and no vibrational evidence of Au−S (~327 cm^{-1}) and Au−Se (~230 cm^{-1}) bond formation was observed, the appearance of acidic protons in TAuSe-311 (Figure 1a), TAuSe-211 (Figure 1b), TAuS-311 (Figure 3a), and TAuS-211 (Figure 3b) strongly implies that the overall reaction may involve hydrolysis, most likely in the form

$$[TOA][Au(III)Br_4] + \frac{1}{2}RX{-}XR + H_2O \rightarrow [TOA][Au(II)Br_3]^- + RXOH + Br^- + H^+ \quad (1)$$

where X is Se or S. However, the Se−Se bond was more reactive than the S−S bond.

The last step in the BSM two-phase synthesis of NPs is the reduction of Au ions by aqueous solution of $NaBH_4$. The TEM images of the Au NPs obtained by adding 10 equiv of $NaBH_4$ to TAuS-311/-311C and TAuSe-311/-311C are presented in Figure 7. The difference between the two samples for a given pair is that one of them had encapsulated water and the other did not. As can be seen clearly in Figure 7, the intermediates formed in the presence of encapsulated water led to the formation of Au NPs of much higher quality in terms of size distribution. We speculate that reaction 1 may lead to a more homogeneous chemical environment compared to breaking the dichalcogenide bond during the formation of metal NPs, of which the latter may lead to the coexistence of different forms of chalcogen-containing species. As shown previously, the coexistence of different forms of chalcogen-containing species during the formation of NPs increases polydispersity of formed NPs.[8,22]

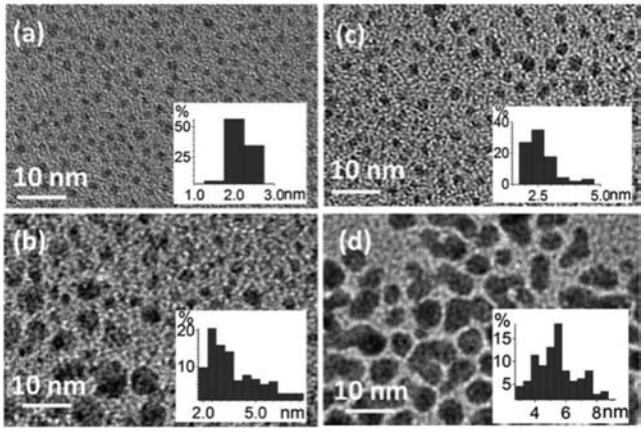

Figure 7. TEM images and corresponding size distribution histograms of Au NPs by adding aqueous solution of 10 equiv of $NaBH_4$ to (a) TAuS-311, (b) TAuS-311C, (c) TAuSe-311, and (d) TAuSe-311C. The respective average sizes are (a) 1.9 ± 0.3 nm, (b) 3.64 ± 1.6 nm, (c) 2.43 ± 0.8 nm, and (d) 5.77 ± 2.1 nm, respectively.

CONCLUSIONS

In summary, we have identified unambiguously that it is the inverse-micelle-encapsulated water that enabled *uniquely* the bond breaking reaction of diselenide or disulfide with Au cations, leading to the formation of a new species that was neither Au(III) nor Au(I) (Figures 5 and 6), which we speculate to be Au(II), and the production of higher-quality Au NPs (Figure 7a and Figure 7c). We have also unraveled some subtle differences in chemistry involving dialkyl diselenide vs disulfide in interaction with Au cations. For instance, the former could form $Au(III)(SeC_4H_9)_2$-like Lewis adduct species but not the latter and the bond-breaking was complete for the former but only partially for the latter. These findings should have important practical ramifications in terms of synthesizing organochalcogen-containing (particularly Se- or Te-containing) ligand-stabilized homogeneous Au metal NPs. Moreover, the inverse-micelle-encapsulated water-enabled bond-breaking chemistry in dialkyl diselenide and dialkyl disulfide may also have implications in biochemical processes involving like species.[24]

ASSOCIATED CONTENT

Supporting Information

Full Raman spectra and DFT molecular structures. This material is available free of charge via the Internet at http://pubs.acs.org.

AUTHOR INFORMATION

Corresponding Author

yyt@georgetown.edu

Present Address

[§]Department of Medicine, Georgetown University Medical Center, 3800 Reservoir Road, NW, Washington, D.C. 20007.

Notes

The authors declare no competing financial interest.

■ ACKNOWLEDGMENTS

The authors thank the UMD NISP lab for use of its TEM facility. The authors thank Allan Cardenas for assistance in EPR measurements. A portion of the research was performed using EMSL, a national scientific user facility sponsored by the Department of Energy's Office of Biological and Environmental Research and located at Pacific Northwest National Laboratory. This work has been funded by NSF (Grant CHE-0923910) and DOE (Grant DE-FG02-07ER15895).

■ REFERENCES

(1) Brust, M.; Walker, M.; Bethell, D.; Schiffrin, D. J.; Whyman, R. *J. Chem. Soc., Chem. Comm.* **1994**, 801.
(2) Sardar, R.; Funston, A. M.; Mulvaney, P.; Murray, R. W. *Langmuir* **2009**, *25*, 13840.
(3) Li, Y.; Silverton, L. C.; Haasch, R.; Tong, Y. Y. *Langmuir* **2008**, *24*, 7048.
(4) Zelakiewicz, B. S.; Lica, G. C.; Deacon, M. L.; Tong, Y. Y. *J. Am. Chem. Soc.* **2004**, *126*, 10053.
(5) Daniel, M.-C.; Astruc, D. *Chem. Rev.* **2003**, *104*, 293.
(6) Hostetler, M. J.; Wingate, J. E.; Zhong, C.-J.; Harris, J. E.; Vachet, R. W.; Clark, M. R.; Londono, J. D.; Green, S. J.; Stokes, J. J.; Wignall, G. D.; Glish, G. L.; Porter, M. D.; Evans, N. D.; Murray, R. W. *Langmuir* **1998**, *14*, 17.
(7) Li, Y.; Zaluzhna, O.; Xu, B.; Gao, Y.; Modest, J. M.; Tong, Y. Y. J. *J. Am. Chem. Soc.* **2011**, *133*, 2092.
(8) Li, Y.; Zaluzhna, O.; Tong, Y. Y. J. *Chem. Commun.* **2011**, *47*, 6033.
(9) Jin, R. *Nanoscale* **2010**, *2*, 343.
(10) Goulet, P. J. G.; Lennox, R. B. *J. Am. Chem. Soc.* **2010**, *132*, 9582.
(11) Li, Y.; Zaluzhna, O.; Tong, Y. Y. J. *Langmuir* **2011**, *27*, 7366.
(12) Matthiesen, J. E.; Jose, D.; Sorensen, C. M.; Klabunde, K. J. *J. Am. Chem. Soc.* **2012**, *134*, 9376−9379.
(13) Jose, D.; Matthiesen, J. E.; Parsons, C.; Sorensen, C. M.; Klabunde, K. J. *J. Phys. Chem. Lett.* **2012**, *3*, 885.
(14) Nuzzo, R. G.; Allara, D. L. *J. Am. Chem. Soc.* **1983**, *105*, 4481.
(15) Brust, M.; Stuhr-Hansen, N.; Nørgaard, K.; Christensen, J. B.; Nielsen, L. K.; Bjørnholm, T. *Nano Lett* **2001**, *1*, 189.
(16) Yee, C. K.; Ulman, A.; Ruiz, J. D.; Parikh, A.; White, H.; Rafailovich, M. *Langmuir* **2003**, *19*, 9450.
(17) Kirihara, M.; Asai, Y.; Ogawa, S.; Noguchi, T.; Hatano, A.; Hirai, Y. *Synthesis* **2007**, 3286.
(18) Deacon, M. L.; Zelakiewicz, B. S.; Tong, Y. Y. *Synlett* **2005**, 1618.
(19) Braunstein, P.; Clark, J. J. H. *J. Chem. Soc., Dalton Trans.* **1973**, 1845.
(20) Gordon, M. S.; Schmidt, M. W. In *Theory and Applications of Computational Chemistry, the First Forty Years*; Dykstra, C. E., Frenking, G., Kim, K. S., Scuseria, G. E., Eds.; Elsevier: Amsterdam, 2005; Chapter 41, p 1167.
(21) *NIST Computational Chemistry Comparison and Benchmark Database, NIST Standard Reference Database Number 101*, release 15b; Johnson, R. D., III, Ed.; National Institute of Standards and Technology: Gaithersburg, MD, August, 2011; http://cccbdb.nist.gov/.
(22) Zaluzhna, O.; Li, Y.; Zangmeister, C.; Allison, T. C.; Tong, Y. Y. J. *Chem. Commun.* **2012**, *48*, 362.
(23) Huang, D.; Zhang, X.; McInnes, E. J. L.; McMaster, J.; Blake, A. J.; Davies, E. S.; Wolowska, J.; Wilson, C.; Schröder, M. *Inorg. Chem.* **2008**, *47*, 9919.
(24) Wessjohann, L. A.; Schneider, A.; Abbas, M.; Brandt, W. *Biol. Chem.* **2007**, *388*, 997.